

Unconventional measurement methods and simulation of aerogel assisted thermoregulation

*Mohanapriya Venkataraman**

Jiří Militký

Rajesh Mishra

Department of Material Engineering, Faculty of Textile Engineering, Technical University of Liberec, Czech Republic.

Soňa Jandová

Technical University of Liberec, Czech Republic.

**mohana.prasad@gmail.com*

ABSTRACT

Aerogels characterized as a low density solid, low optical index of refraction, low thermal conductivity, and low speed of sound through materials, high surface area, and low dielectric constant. It has super-insulating characteristics and the heat transfer phenomenon associated with its complex nanoporous structure. Overall, it delivers better thermal performance, improved durability, and faster installation times than the incumbent insulation materials. Due to these advantages, aerogel is used in many industries like manufacturing, oil & gas, automotive, textiles, construction etc., for steam distribution and thermal insulation application. Measurement of thermal properties of aerogel coated material is important to evaluate its usefulness under extreme weather condition. This study was focused on thermal insulation of aerogel coated high performance fibrous materials. Various measurement techniques for different combinations of insulation materials were studied. New methods were explored to measure thermal characteristics at extreme temperatures. Further, a few instruments were to be fabricated to measure and correlate thermal properties at sub-zero temperatures. This study was expected to assist in identifying the optimal thermal measurement technique and the insulation material most suitable for use. The results from the new measurement techniques like PIV and laboratory set-up instrument will be relevant for classification of materials and eventually for quality assessment of all type of insulation materials. Modeling and simulation were used to study the heat transfer

through porous aerogel materials. The thermal resistances of samples were found to be directly proportional to its thickness. This may be attributed to decrease in heat losses due to space insulated by fibrous structure and nanoporous aerogel structure. The air permeability was found to be directly proportional to percentage of nanoporosity of the aerogel based fibrous structure. The fabric density and the aerogel present in the fabric have a significant effect on thermal properties of the overall structures. Compared to other materials, the aerogel-based samples were found to have considerably high thermal resistance even at extreme temperatures.

Keywords: *Aerogel, Thermal Insulation, High Performance fabrics, Nanoporous structures.*

Introduction

Combination of different types of fabrics, with various coatings and treatments, are being studied to understand and improve the effectiveness of materials as thermal insulators. Different kinds of fibrous materials such as traditional nonwovens are used as the middle thermal insulating layer. Nonwoven fabrics are important components for good thermal insulation from the surroundings, and they offer both space and weight savings[1]. The important constructive parameters are thickness, weight per unit area and packing fraction p.f., which is the ratio between the bulk density of fibrous structure samples and of the same sample if it was made up wholly from the same polymer [2]. Thermal insulation properties are determined by the physical parameters of fibrous structures as well as the structural parameters [3].

Heat is usually referred to in thermodynamics through the term “heat transfer”, which is consistent with the ability of heat to raise or lower the energy within a system. Since fabric is a heterogeneous system of air and fabric, conduction through air and fibers contributes to total thermal conduction of the fabric [4]. All three modes of heat flow rely on a temperature difference for the transfer of energy to take place. The greater the temperature difference the more rapidly will the heat be transferred [5]. The function of insulation materials is to minimize the transport of heat through the construction. The insulation materials are highly porous with small amount of solid structure. In a material with a small amount of solid, the importance of the radiation will increase. This creates an optimal point from insulation perspective, for a certain material, where the sum of the contributions from radiation and solid conduction is at a minimum. This sum will add to the gas conduction which for conventional insulation materials can be considered as constant. This gives a total thermal conduction down to a minimum around 0.03 W/(mK), which can be compared to the air conductivity of 0.025 W/(mK). The passage of thermal energy through an

insulating material occurs through three mechanisms: solid conductivity, gaseous conductivity, and radiative (infrared) transmission. The sum of these three components gives the total thermal conductivity of the material. Solid conductivity is an intrinsic property of a specific material. The improvement of thermal resistance of the fabric can be achieved by decreasing the thermal conductivity. Fricke et al. observed that both the solid conductivity and the gas conductivity were proportional to the density as shown below:

$$\lambda_{\text{gas}} : \rho^{-0.6} \quad (1)$$

$$\lambda_{\text{solid}} : \rho^{1.5} \quad (2)$$

Hummer et al. using these relations derived the following relation for the radiative conductivity, which is a relative equation for the thermal conductivity of opacified silica aerogel:

$$\lambda_{\text{total}}(\rho) = \lambda_{\text{solid}} \left(\frac{\rho}{\rho_0} \right)^{1.5} + \lambda_{\text{gas}} \left(\frac{\rho}{\rho_0} \right)^{-0.6} + \lambda_{\text{rad}} \left(\frac{\rho}{\rho_0} \right)^{-1} \left(\frac{T}{T_0} \right)^3 \quad (3)$$

where ρ (kg/m^3) is the density; λ_{total} , λ_{gas} , λ_{solid} , and λ_{rad} [$\text{W}/(\text{mK})$] are the total conductivity, the conductivity for gas conduction, the conductivity for solid conduction, and the radiative conductivity, respectively; T ($^{\circ}\text{K}$) is the temperature, and the index 0 means that parameters are related to a reference material from an aerogel [6]. Aerogel is made of more than 90% of air, having extremely low weight, transparency, and excellent thermal conductivity. Aerogel is an ideal material for thermal insulation due to all these properties [7, 8]. However, silica aerogel possess a very small (~1 to 10%) fraction of solid silica with pore diameters in the range of 10 to 100 nm. Additionally, the solids that are present consist of very small particles linked in a three-dimensional network with many "dead-ends". Therefore, thermal transport through the solid portion of silica aerogel occurs through a very tortuous path and is not particularly effective. Further decrease in thermal conductivity of aerogel can be observed if evacuated below 50 hPa; thermal conductivity decreased because of elimination of pore gas. Super insulations with extremely low thermal conductivities can be implemented with evacuated highly porous powder, fiber, or gel spacers. Due to the Knudsen effect, thermal conductivity can become lower than that for the still air, that is, even less than 25 [$\text{mW}/(\text{mK})$][9]. Heat transfer phenomenon in silica aerogel is associated with its complex nanoporous structure [10, 11]. The porosity is more than 90% with a thermal conductivity lower than that of air, which makes these aerogel a highly insulating material. The pores of silica aerogel are open and allow the passage of gas through the material[6]. Soleimani Dorcheh and Abbasi reported the synthesis of nanostructured silicon based transparent aerogel with pore diameter 20 to 40 nm [12].

Aerogel are characterized with a very low permeability which can be explained in terms of pore size suitable for transport of water vapors/gases but not for water molecules [13].

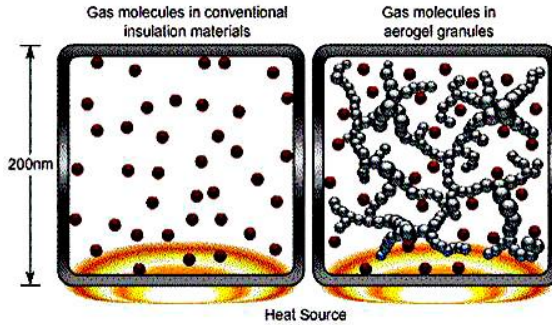


Figure 1. Gas molecules in conventional insulation material and aerogel granules [9].

A number of instruments have been developed for measurement of thermal properties. These instruments can broadly be categorized as steady state measurement and transient measurement devices. Thermal resistance is commonly measured using steady state method and thermal diffusivity in the transient state method. Study of recent developments show that further studies have been conducted to understand the transient properties of fabrics than the steady state aspects. Hence, sweating plates and copper manikins are being increasingly used instead of simple hot plate or cylindrical devices. However, a measurement based on the standardized steady-state dry heat transfer method has its own advantages in experimental simplicity and low equipment cost[14].

This study is focused on thermal insulation of aerogel coated high performance fibrous materials. Various measurement techniques for different combinations of insulation materials were studied. New methods were explored to measure thermal characteristics at extreme temperatures. Further, a few instruments were to be fabricated to measure and correlate thermal properties at sub-zero temperatures. This study could help in identifying the optimal thermal measurement technique and the insulation material most suitable for use.

Materials and Methods

Materials

In this study, 50:50 ratio compositions of six polyester/polyethylene non-woven fabrics treated with aerogel were used. Polyester is the most versatile,

most cost effective and most widely used fiber in various applications. It is perfect for any application where a flexible non-woven fabric is required. It is also often supplied as the waterproof material and insulator for the winter clothing. It retains the physical properties when wet and stays extremely stable during humidity changes. This strong and light material resists moisture, staining and chemical attack. Polyethylene has excellent chemical resistant, impact strength and electrical properties, as well as low water absorption, this tough and flexible material is ideal for non-toxic skin contact, and is perfect for clothing. The type of aerogel used was hydrophobic amorphous silica aerogel which is most suitable for application in textile material which provides the super insulating properties of silica aerogel in a flexible form. It is excellent for ambient and sub-ambient insulating applications. The aerogel particles were added during thermal bonding of the non-woven web. The samples were chosen in six different thicknesses as are widely used in most textile insulating applications. These thicknesses are commonly used for insulation of clothing, tents and buildings. Sample H1 is Needle punched struto nonwoven structure having One layer of PP web (Top layer) + One layer of spunbond PP web having melt blown polyamide nanofibers on both sides (Middle layer)+One layer of PP web (Bottom layer). Sample H2 is Needle punched struto nonwoven structure having one layer of PP web (Top layer)+ Two layers of spunbond PP web having meltblown polyamide nanofibers on both sides (Middle layer)+One layer of PP web (Bottom layer). Sample M1 was purchased from Elastic Gros Braun patent no. M123A2046 and Sample M2 were purchased from POLARTEC with 100% polyester and 100 gsm alpha insulation. Silica aerogel powder and granules were purchased from Cabot aerogel Corp. Polyurethane (PUR) and PolyvinylideneFlouride (PVDF) was used from the CxI lab (nanocenter, TUL, Czech Republic). To obtain an indication of the effect of areal density on thermal properties, fabrics with comparable densities in different thicknesses and their corresponding weights were measured. The density difference in samples may be attributed to the fabric structure and also in aerogel treated nonwoven fabrics the percentage of aerogel particles present in the fiber. Approximate volume porosity of all aerogel treated samples was around 93%. Since the fabric samples were created from multilayer nonwoven structures and it is complicated to calculate mean fiber density. Fabric density (kg/m^3) is calculated as ratio of mass per unit area [G (g/m^2)] and thickness [h (m)].

$$\text{Fabric density} = \frac{G}{h} \text{ [kg/m}^3\text{]} \quad (4)$$

Table 1. Description of samples.

Sample No.	Sample description	Thickness [mm]	Weight [g/m ²]	Fabric density [kg/m ³]
S1	Aerogel treated nonwoven fabrics	3.42	272.56	79.66
S2	Aerogel treated nonwoven fabrics	6.21	499.46	80.42
S3	Aerogel treated nonwoven fabrics	6.61	440.70	66.73
S4	Aerogel treated nonwoven fabrics	8.06	535.10	66.39
S5	Aerogel treated nonwoven fabrics	11.12	733.7	65.99
S6	Aerogel treated nonwoven fabrics	13.80	942.70	68.33
H1	Needle punched struto nonwoven structure	9.34	402.01	43.06
H2	Needle punched struto nonwoven structure	8.05	407.50	50.64
M1	Elastic Gros Braun patent no. M123A2046	1.85	101.80	55.20
M2	POLARTEC with 100% polyester and 100 gsm alpha insulation	1.52	104.13	68.39

Note: “±” is the upper and lower 95% confidence interval of the mean.

Method and Parameters of Sample Preparation

The aerogel treated nonwoven fabrics were produced by thermal bonding. The confocal microscopic image of aerogel treated nonwoven fabric is shown in figure 2. The fibers for the thermal bonding were selected based on the thermal properties and glass transition temperature. Polyester (T_g -161.7°C for density-1.3584 g/cc) has the higher glass transition temperature than Polyethylene fibers (T_g - 85°C). The properties of amorphous silica aerogel are shown in table 2.

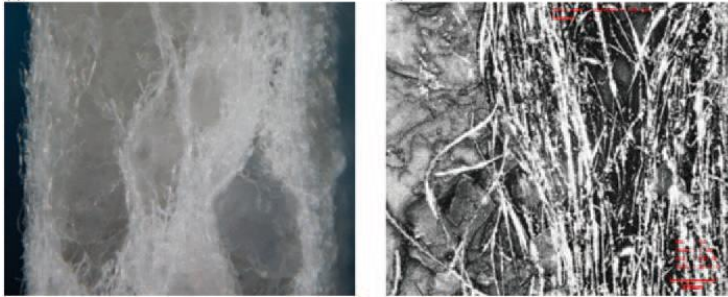


Figure 2. Confocal microscopic image of aerogel treated nonwoven fabric.

Table 2. Properties of amorphous silica aerogel.

S. No.	Properties	Value range
1	Particle size range	0.1 to 0.7mm
2	Pore diameter	~20 nm
3	Particle density	120 to 140 [kg/m ³]
4	Surface chemistry	Fully hydrophobic
5	Thermal conductivity	0.012 [W/(m K)] at 25°C

Needle punched struto nonwoven fabrics were produced in our faculty. The polypropylene (PP) web and melt blown polyamide nanofibers were produced separately and were bonded together by needle punched struto nonwoven fabric machine shown in figure 3.

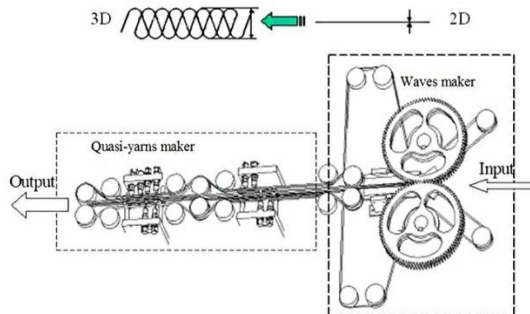


Figure 3. Schematic diagram of needle punched struto nonwoven fabric machine.

The fabric is in the form of corrugated structure where top and bottom layer is polypropylene web and the middle layer consists of melt blown polyamide nanofibers on both sides of spunbond PP web with two different compositions.

Measurement Methods

Before conducting the measurements, all samples were conditioned at standard atmospheric conditions ($20 \pm 2^\circ\text{C}$, $65 \pm 2\%$ R.H) for 24 h. The non-woven fabric samples were characterized using SEM (VEGA TESCAN Inc. USA) at 30 kV and confocal microscope (OLYMPUS Confocal Scanning IR Laser Microscope, LEXT LS3000-IR).

BET instrument was used for determining aerogel porosity. In this technique a gas, usually nitrogen, at its boiling point, is adsorbed on the solid sample. The amount of gas adsorbed depends of the size of the pores within the sample and on the partial pressure of the gas relative to its saturation pressure. By measuring the volume of gas adsorbed at a particular partial pressure, the Brunauer, Emmitt and Teller (BET) equation gives the specific surface area of the material. At high partial pressures, where there is hysteresis in the adsorption/desorption curves (called "isotherms"), the Kelvin equation gives the pore size distribution of the sample. The pore size distribution is determined using a 40-point nitrogen adsorption/desorption analysis. Gas adsorption methods are generally applicable to pore in the mesopore range. However, microporosity information can be inferred through mathematical analyses such as t-plots or the Dubinin-Radushevich method. Gas adsorption cannot effectively determine macropores. Autosorb IQ MP Quantachrome Instrument, USA was used to evaluate the method of adsorption of nitrogen at liquid nitrogen temperature and the evaluation was performed by the software provided by Autosorb IQ MP Quantachrome Instruments using gas adsorption/desorption method. According to the firmware, a standard procedure was used for determining the specific surface area by adsorption of nitrogen using multipoint BET method and the analysis of nitrogen adsorption/desorption curve at liquid nitrogen temperature.

Measurement of Thermal Properties

Particle Image Velocimetry (PIV) is a whole-flow-field technique providing instantaneous velocity vector measurements in a cross-section of a flow. Two velocity components are measured, but use of a stereoscopic approach permits all three velocity components to be recorded, resulting in instantaneous 3D velocity vectors for the whole area. The use of modern digital cameras and dedicated computing hardware, results in real-time velocity maps. In normal PIV systems, the chamber set-up was very big and the hot plate was not used to determine the thermal properties. In our research, the chamber was made with the dimensions of 10 x 10 cm wide and 70 cm height. Three different set-ups were custom built to measure the velocity profile above the fabric sample shown in figure 4. The first set-up was placing the fabric sample directly on the hot plate. The second and third set-up was to place the fabric sample 2 and 5 cm above the hot plate respectively.

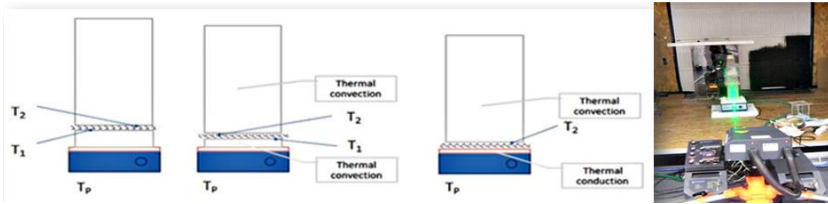


Figure 4: Experimental set-up for PIV measurements.

After the test is performed with the tracer particles for the heat flow, the image captured by the CCD camera is saved in the system. First, the images are divided into small windows called interrogation regions. Using a statistical method called cross-correlation, the displacement of each window from frame 1 to frame 2 is determined from the peak point in the cross correlation function. The most probable displacement over the time interval is the average velocity vector in one interrogation window, i.e. $\Delta x / \Delta t \approx v$, shown in figure 5. By repeating these calculations, the velocity field of the entire image area is obtained.

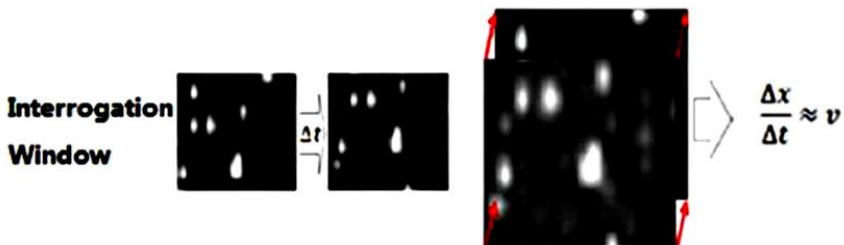


Figure 5: Average velocity vector of one interrogation window obtained by cross correlation[16].

Details of the PIV technique, including the tracer particle size, light source, light sheet optics, digital image recording, post-process data analysis and mathematical background of the statistical PIV evaluation can be found in the state of the art section [17].

The newly fabricated instrument works according to transmission of heat in the steady-state condition as described in BS 4745:1971. Single-plate heating method was used as reference to fabricate this instrument. In single-plate method (figure 6), the specimen under test is placed on the heated lower plate covered with 100% cotton as an outer fabric, since the issue of thermal contact is also very important. Fixed pressure (10 g/cm²) was applied on the test specimen during the measurement which ensures good contact without deformation of textile structure. The surface temperature of the outer fabric is measured using the infrared thermometer.

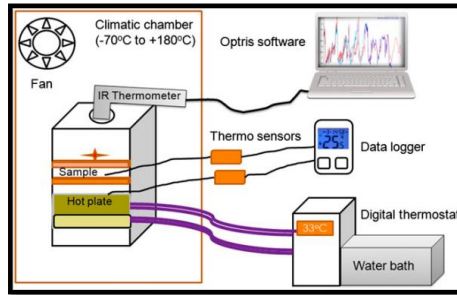


Figure 6: Schematic diagram of custom-built instrument for measuring thermal properties.

The instrument was used to determine the temperatures at various positions on the aerogel-treated fabric. From these measurements, the thermal conductivity and thermal resistance were calculated. The sample was placed in a climatized temperature system (chamber) which operates with the temperature range from (-70 to +180°C). The instrument measures the heat transport through textile material. The test specimen was placed on the cylindrical hot plate which is connected to the digital thermostat water bath where the skin temperature is maintained at ~33°C as shown in figure 7. The test specimen was placed on the hot plate and the outer fabric (100% plain woven cotton fabric) was placed over the test specimen applying 10 g weight on each side. Two thermocouples and heat flow sensors were used to measure temperature variations. First one (T_1) is fixed on the surface of the test specimen which touches the hot plate and the second one (T_2) is fixed on the surface which is covered by the outer fabric. The hot plate was adjusted to constant skin temperature and the climatic temperature system was adjusted to a controlled constant differential temperature. The heat flow sensors act on both the surfaces of the fabric. With the help of thermocouples, the temperature difference between the upper surface and the inner side of the test specimen can be measured. The Infrared thermometer was used to measure the temperature variations on the surface of the outer fabric. The fundamental measuring principle implies the measuring and processing of the heat flows with dependence to time. The instrument measures parameters: (1) Temperature on the surface of the test specimen which is in contact with the skin (T_1), (2) Temperature on the surface of the fabric which is in contact with the outer fabric (T_2), (3) Temperature inside the climatic temperature chamber which is set as the environmental temperature from (+25 to -25°C) (T_3) and (4) Temperature on the surface of the outer fabric which is sensed by infrared thermometer (T_4).

The thermal property of fabrics under heat convection was evaluated by a laboratory model device developed in department of material engineering, Technical University of Liberec, shown in figure 7. This device consists of

one air tunnel, sample holder, heater, several sensors, data acquisition module and laptop. The thermocouples are attached to one to heater and the other to the fabric, and the anemometers are on both sides of fabric, data acquisition module connects sensors with PC. The air flow goes through the testing sample, the temperatures of both sides of the fabric can be real-time monitored and saved in laptop. The output of heater was around 60°C at 2.5 m/s.

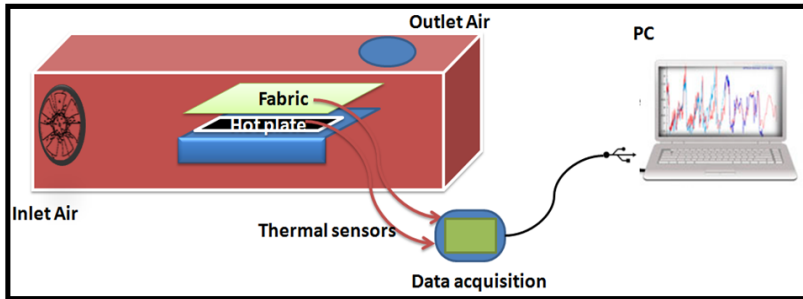


Figure 7: Schematic of laboratory model thermal convection instrument.

Heat energy transfers between a solid and a fluid when there is a temperature difference between them. This is known as "convection heat transfer". The temperature of the solid due to an external field such as fluid buoyancy can induce a fluid motion. This is known as "natural convection" and it is a strong function of the temperature difference between the solid and the fluid. Blowing air over the solid by using external devices such as fans, pumps and even heat generation within the object can also generate a fluid motion which is known as "forced convection". Fluid mechanics plays a major role in determining convection heat transfer.

Computational Simulation of Heat Transfer using ANSYS and COMSOL

The simulation of convective heat transfer through aerogel treated nonwovens was conducted using ANSYS and COMSOL. Two different simulation softwares were used for comparison purposes. The simulation data was used to validate the experimental data generated through other experiments. Also, the heat transfer properties of the fabric can be further optimized with assistance of the models generated through these softwares.

ANSYS Simulation

Before a model is set, it passes through several stages. Thermal analysis is one of them and plays a very important role in product development. Various products such as engines, refrigerators, heat exchangers and so on

are designed based on the results of this analysis. Thermal analysis is used to determine the temperature distribution and related thermal quantities in the model. In this analysis, all heat transfer modes, namely conduction, convection and radiation are analyzed. The output from a thermal analysis are (1)Temperature distribution; (2)Amount of heat loss or gain; (3) Thermal gradients and (4) Thermal fluxes. This analysis is used in many engineering industries such as automobile, piping, electronic, power generation, and so on. In ANSYS workbench, two types of thermal analysis can be carried out, namely Steady-State and transient Thermal Analysis. The steady-state thermal analysis may be either linear or non-linear, with respect to material properties that depend on temperature. The thermal properties of most of the materials do vary with temperature; therefore the analysis usually is non-linear. Including radiation effects or temperature-dependent convection in a model also makes the analysis nonlinear. The steps to solve a problem relate to the thermal analysis are the same as that of the structural analysis, except a few steps such as selecting the element-type, applying the load, and post processing results. In the transient thermal analysis, the system is studied under varying thermal loads with respect to time. The temperatures can be derived varying with time, thermal gradients and thermal fluxes in a transient thermal analysis. The transient thermal analysis takes more time compared to other analysis types. It is necessary to understand the basic mechanism of the problem to reduce the time involved in getting the solution. For example, if the problem contains nonlinearity, then you first need to understand how they affect the response of structures by doing the steady-state thermal analysis. Owing to the highly random structure of non-wovens/sheet/batt, a unit cell was considered. Individual fibers were modeled, each having a circular cross-section and a random shape.

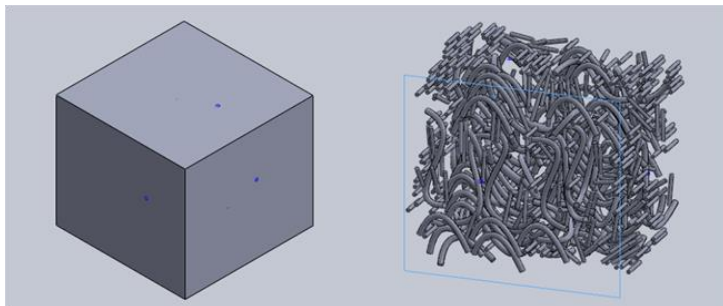


Figure 8: Unit cell model of nonwoven.

For this, a spline (a curve) was made, and the profile of a circle was swept over the spline to create the fiber. The modeled fibers were assembled together to create a nonwoven structure, such that the fibers occupy 26.27% space inside the unit cell, so as to give 73.73% porosity to the fabric as

shown in figure 8. This assembly of fibers was saved as a PART file so that it could be used as a component in the further complex assembly.

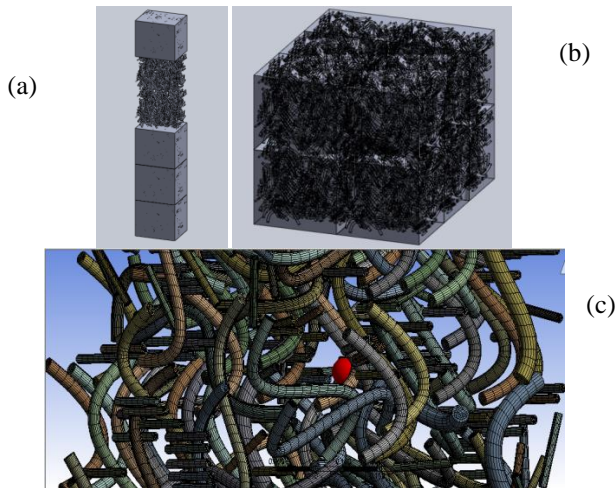


Figure 9: (a) Whole width of the fabric (b) Macroscale image of the nonwoven fabric (c) Meshing of elements in the unit cell

A chain of unit cells, about 3.5 mm long, was assembled using the ‘mate’ function to give a more realistic view of the fabric – this was simulated in ANSYS Workbench 14. A model view of the structure of the non-woven fabric developed has been shown in figure 9.

COMSOL Simulation

A unit cell to represent the fabric sample was modeled in SOLIDWORKS. The fiber percentage in the unit cell was approximately 26.5%. Most of the fiber parts were aligned in the machine direction and very few in other directions as shown in figure 10(a).

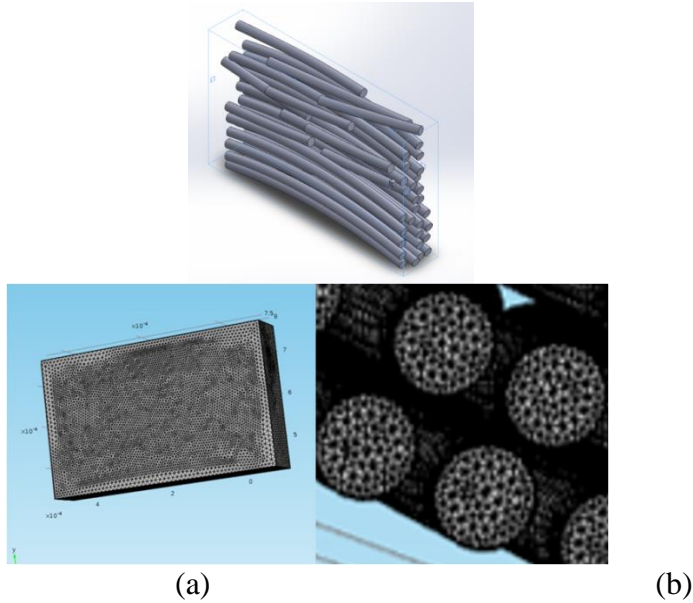


Figure 0. (a) Fiber alignment in the unit cell (b) Meshing of the unit cell.

The simulation of heat transfer through the fabric unit cell was done in COMSOL. The simulation was done assuming laminar and compressible flow and results obtained were for the steady state. One of the faces of the fabric was given a constant temperature of 329.19 K and the outside temperature was taken to be 263.15 K. This was done for 4 cases:(1) Aerogel as the fluid in the fabric with forced convection (2.5 m/s wind at the outer surface); (2) Aerogel as the fluid in the fabric without forced convection. (3) Air as the fluid in the fabric with forced convection (2.5 m/s wind at the outer surface) and (4) Air as the fluid in the fabric without forced convection. The model was meshed and various boundary conditions were given as shown in figure 10(b). For both with and without forced convection cases, one face was given a temperature of 329.19 K and initial temperature of the whole fabric was given as 263.15 K. For the forced convection case, the opposite face was given a convective flux with convection factor 23.76 [W/(m²K)] (2.5 m/s wind) and 263.15 K outside temperature. For the case without forced convection, the opposite face was given an open boundary condition with outside temperature of 263.15 K. The meshing parameters are as given in Table 3.

Table 3. Meshing Parameters

Parameter	Value
Maximum size given	5.7×10^{-5} m
Minimum size given	1.03×10^{-5} m
Boundary layer thickness	5.7×10^{-6} m
Number of mesh elements total	1816188.

Results & Discussions

Microscopic Analysis of Samples

Results for the characterization of aerogel treated nonwoven fabrics and needle punched struto nonwoven structure samples by SEM, Confocal/optical microscopy, DSC, FTIR and BET analysis as confirmation techniques are discussed. The aerogel deposition in the fabric between the fibers was also observed. Figure 2 shows the images taken from confocal microscope. The aerogel particles present between the fibers can be seen clearly from the images. The inter-fiber spaces are clearly visible. The micro spacing between fibers is filled with aerogel particles. It can be seen that the aerogel is covering surface of individual fibers and is uniformly distributed in the structure. SEM images are shown in figure 11. The aerogel deposition on the fibers can be clearly observed. These images provide a more clear understanding of the deposition of silica aerogel particles on the fiber surface. Fiber arrangement plays a vital role in deciding the density and thus the porosity of nonwoven fabrics. The fabric is in the form of corrugated structure where top and bottom layer is polypropylene web and the middle layer consists of melt blown polyamide nanofibers on both sides of spunbond PP web shown in figure 12.

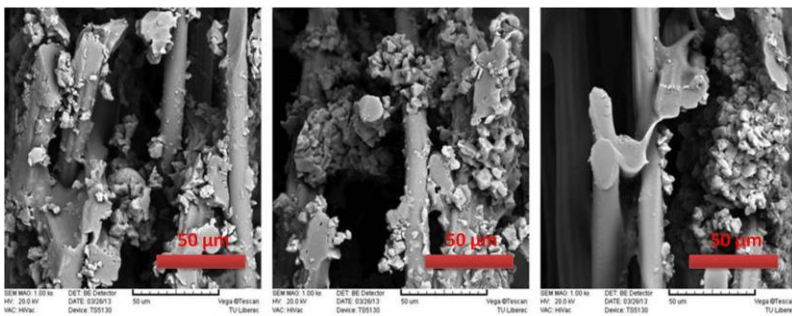


Figure 11: Scanning electron microscope images of aerogel-treated nonwoven fabrics.

Needlepunched Struto Nonwoven Sample

The struto fabric shown in the figure 12 is in the form of corrugated structure where top and bottom layer is of polypropylene web and the middle layer consists of melt blown polyamide nanofibers on both sides of spunbond PP web with two different compositions.

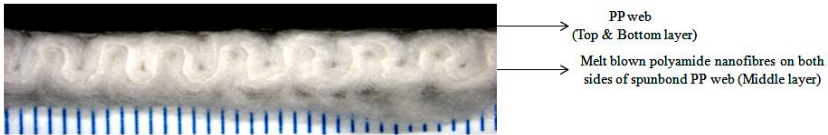


Figure 12. Needle punched struto nonwoven structure.

Gas Adsorption/Desorption of SiO₂ Aerogel Particles

The pore structure of silica aerogel is difficult to describe by geometry. The International Union of Pure and Applied Chemistry has recommended a classification for porous materials where pores of less than 2 nm in diameter are termed "micropores", those with diameters between 2 and 50 nm are termed "mesopores", and those greater than 50 nm in diameter are termed "macropores". Silica aerogel possess pores of all three sizes. However, the majority of the pores fall in the mesopore regime, with relatively few micropores[18-20]. It is very important when interpreting porosity data to indicate the method used to determine the data. Nitrogen adsorption/desorption method was used for determining aerogel porosity. In this technique a gas, usually nitrogen, at its boiling point, is adsorbed on the solid sample. The amount of gas adsorbed depends on the size of the pores within the sample and on the partial pressure of the gas relative to its saturation pressure. By measuring the volume of gas adsorbed at a particular partial pressure, the Brunauer, Emmitt and Teller (BET) equation gives the specific surface area of the material. At high partial pressures, where there is hysteresis in the adsorption/desorption curves (called "isotherms"); the Kelvin equation gives the pore size distribution of the sample. The pore size distribution shown in figure 13 was determined using a 40-point nitrogen adsorption/desorption analysis. Gas adsorption methods are generally applicable to pore in the mesopore range. However, microporosity information is inferred through mathematical analyses such as t-plots method. Gas adsorption cannot effectively determine macropores.

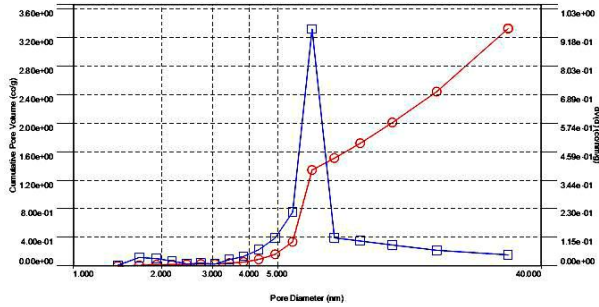


Figure 13: Distribution curve of pore diameter and cumulative pore volume curve for aerogel sample.

The nitrogen sorption experiments performed for the methyl functionalized silica aerogel resulted into specific surface areas. Amorphous silica aerogel in granular form was measured for the surface area and porosity. The measured total specific surface (BET) area A was $783 \text{ m}^2/\text{g}$ (correlation coefficient of 0.9999) and total pore volume ($d < 40 \text{ nm}$) $V_v = 2.686 \text{ cm}^3/\text{g}$. The micropores diameter was $d < 2 \text{ nm}$ which was measured by t-plot method according to de Boer. The specific surface area ' A ' micro was $0 \text{ m}^2/\text{g}$ and the pore volume V micro was $0 \text{ cm}^3/\text{g}$. The mesopores measured by BJH method from the desorption branch of the isotherm is shown in figure 13, the assumption is cylindrical pores. Figure 13 shows distribution curve of pore diameter and cumulative pore volume curve for aerogel sample (assuming cylindrical pores) from the desorption branch of the isotherm; x-axis is pore diameter in nm.

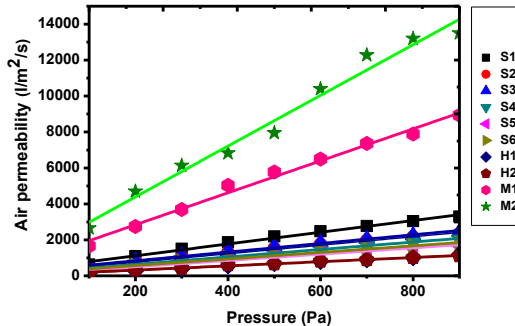


Figure 14: Flow rate dependence on pressure.

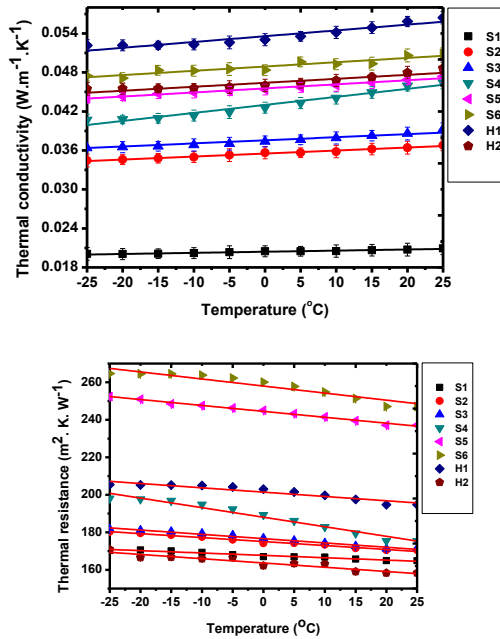
Air permeability is the measure of airflow passed through a given area of a fabric. This parameter influences the thermal comfort properties of fabrics to a large extent. It is generally accepted that the air permeability of a fabric

depends on its air porosity, which in turn influences its openness. With more porosity, more permeable fabric is obtained. Statistical analysis results show that there is a significance on the air permeability values of the aerogel treated nonwoven fabrics ($p = 0.003$). Figure 14 shows the air permeability with respect to different pressure levels of the fabrics. The result indicates that air permeability is directly proportional to the pressure level. On comparison of ten fabrics, the air permeability is higher in the case of sample M2. It may be due to the fact that air permeability is related to porous structure of the fabric and is directly proportional to percentage of porosity of the fabric. It was also noticed that when the pressure level increased, the flow rate also increased. Irrespective of different pressure levels, the air permeability was low for samples S1 to H2. It may be attributed to the layered structure and high porosity.

Evaluation of Thermal Properties by Custom Built Equipment

Effect of Temperature Variations

The environmental temperature versus the thermal conductivity of the fabric is shown in figure 15. The temperature variations at each point varied for the test specimens with the change in climatic chamber temperature (environmental temperature). The temperature gradient was higher for the lower temperatures (sub-zero temperatures). The temperature of materials is determined with thermal energy in the form of kinetic energy of disordered molecular movement [21]. Temperature gradient is an important factor for calculating the thermal conductivity of the test specimens. This difference in temperature gradient may be attributed to the aerogel present in the non-woven fabric. Aerogel is the main component in the non-woven fabric structure blocking air pockets inside its highly porous structure which provides thermal insulation and thereby considered to be beneficial for such applications. In the initial stage of exposure, it was found that the fabric temperature variations increased rapidly. This may be because of the temperature difference between the fabric sample and the exposed air is high in the early stage of the exposure process. As the temperature stabilized, the variations decreased. It can be observed that the temperature difference between the inner surface and outer surface of test specimen increased as the sample thickness increased. A bulkier sample with lower density and more air pores inside proved to be more efficient in insulating the flow of heat from the hot plate to outer environment. It means that a human body can maintain the skin temperature for a longer time with insulating material of higher thickness having higher porosity. Aerogel treated samples performed better in thermal insulation as compared to other samples at extreme temperatures. The F-test was done for all the samples and the adjusted R-Square was around 0.95 for all the samples.



(a) (b)
Figure 15: Custom built Instrument (a) Thermal conductivity (b) Thermal resistance

Thermal conductivity increases with fabric density and also for constant thickness of fabric; and below density of 60 kg/m^3 , increase in fabric thickness causes increased thermal insulation and reduction in fabric temperature variations (up to an optimum level). The increase in weight-to-thickness ratio causes increase in effective thermal conductivity due to increase in fiber-to-fiber contact and packing density. It causes increase in tortuosity i.e. mean free path for photons to be travelled and so less heat flows through the channels in nonwoven fabric [22, 23]. Regardless of the shape of the material, aerogel-treated non-woven fabric acts as an insulating layer with a conductivity that is constant. From figure 15(a), it can be seen that the thermal conductivity of the samples didn't show significant difference with respect to environmental temperature. Due to the open pore structure and irregular pore network of the aerogel present in fabric, solid and gaseous thermal conductivity is reduced. This reduction is due to the Knudsen effect, where the excited gas molecules that are entering the open pore structure of the silica aerogel collide with the surface of the aerogel and transfer their energy to the surface [24]. This reduces the gaseous movement, thus limiting the silica aerogel's gaseous thermal conductivity. Gaseous

thermal conductivity can also be reduced by 33% by placing the aerogel under vacuum [25]. Sample S1 showed lower conductivity compared to other samples due to a relatively higher percentage of aerogel content.

Determination of Thermal Resistance at Various Temperatures

Figure 15(b) demonstrates how the environmental temperature affects the result in an almost linear relation between fabric thickness (expressed as volume of insulation material per unit of fabric area) and insulation [26]. Uniform distribution of heat provides the best insulation in the extreme cold conditions. Thermal insulation increases with thickness due to increased quantity of enclosed air, whereas if thickness is maintained constant, then thermal insulation decreases with increase in weight as quantity of enclosed air is reduced [27]. The thermal insulation value of porous, low-density non-woven fabric is affected by compression and hence the layered structure of aerogel treated non-woven fabric gives better insulation because of good compression recoverability. It can be observed that samples S2, S3, S4, S5 and S6 have higher resistance when compared to sample S1, H1 and H2. Thus, it can be stated that thickness and aerogel present had more profound effect on insulation compared to the material composition. One interesting observation is that the thermal resistance is higher at lower temperatures, in spite of having almost similar conductivity at all temperatures (51). This is mainly attributed to the nature of nanopores of air in the structure which are capable of higher insulation at much higher temperature gradient. However, after certain level of stabilization, their heat insulation capacity goes down and the resistance is also visibly lower. It was examined by one-way analysis of variance (ANOVA) with 95% confidence level. A significant difference ($p < 0.05$) has been observed. The analysis of variance (ANOVA) result reported as an F-statistic and its associated degrees of freedom with significance limit (p value). Here, the ANOVA F-statistic is a ratio of variation between groups and variation within group. The F-test was done for all the samples and the adjusted R-Square was around 0.95 for all the samples. A large F is evidence against H_0 (null hypothesis), since it indicates that there is more difference between groups than within groups. ANOVA was done to analyze the results with 95% confidence level. A significant difference ($p < 0.05$) has been observed in the thermal resistance and conductivity properties of the nonwoven fabrics with different thicknesses.

Effect of Aerogel on Thermal Insulation of Fabrics

The influence of wind speed on the thermal insulation properties of the fabrics has been studied. It is expressed as a percentage which represents the reduction in the rate of heat loss due to the insulation, relative to the heat loss from the surface. If figures 17(a) and 17(b) are considered, it can be observed that heat retention properties is always more important for fabrics in colder environments; besides there is a linear relationship with the air flow velocity.

The fabrics with high porosity will prevent air passage and then reduce convection heat loss. The F-test was done for all the samples and the adjusted R-Square was between 0.8 and 0.90 for all the samples.

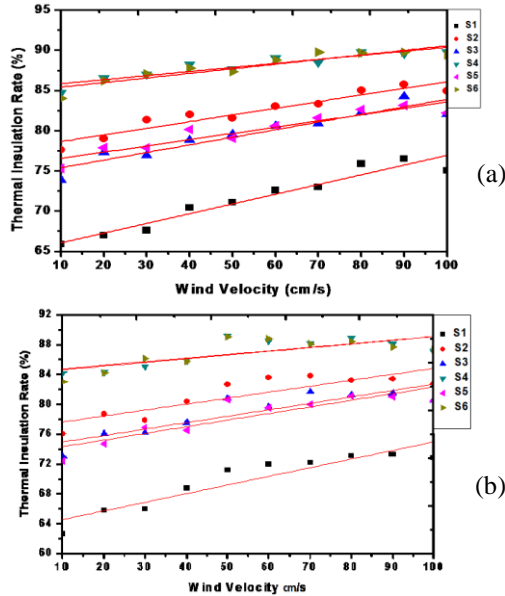


Figure 16: Thermal Insulation of fabrics (a) KES Thermolabo II (b) NT-H1

It is observed from figure 16(a) and 16(b) that with the increase in aerogel content, the thermal insulation rate increases with increase in wind velocity. This may be attributed to higher thickness of the fabric having higher aerogel content. All data were analyzed and found to fit the linear regression model. The residuals approximates (independent random errors) and goodness of fit (coefficient of determination, R^2), were calculated to see how closely values obtained from fitting a model match the dependent variable the model is intended to predict. The calculated results showed closer fit to data (goodness of fit was closer to 1 ($R^2=1$)).

Validation of Theoretical Model with Experimental Data

The correlations between experimental and theoretical model data are show in the figures 18 to 21. Theoretical model data was correlated with the measured data of three instruments namely, alambeta, TCi and custom built instrument. The theoretical model data were calculated as per the formulae given below. The thermal conductivity of parallel arrangement λ_{hp} (higher limit) is equal to,

$$\lambda_{hp} = P \lambda_a + (1 - P) \lambda_f \quad (5)$$

For serial arrangements is thermal conductivity λ_{hs} (lower limit) defined as

$$\lambda_{hs} = \frac{\lambda_a \lambda_f}{P \lambda_f + (1-P) \lambda_a} \quad (6)$$

Actual composition of a fibers and air phases can be presented by linear combination of parallel and series structures [28]. The compromise is to compute the mean thermal conductivity of hollow fiber λ_h as arithmetic mean between upper and lower limit.

$$\lambda_h = \frac{\lambda_{hP} + \lambda_{hS}}{2} \quad (7)$$

The parallel/series structure gives a firsthand prediction and would give reasonable prediction accuracy for practical application due to its simplicity. From the figure 17 to 20, it can be seen that the correlation between the theoretical and experimental values of thermal resistance were around $R^2 = 0.8$ for alambda and custom built instrument. Around $R^2= 0.9$ was for TCi instrument. Since the correlation between the theoretical calculation and the experimental values are good, it can be concluded that the data generated from the experiments are theoretically compatible.

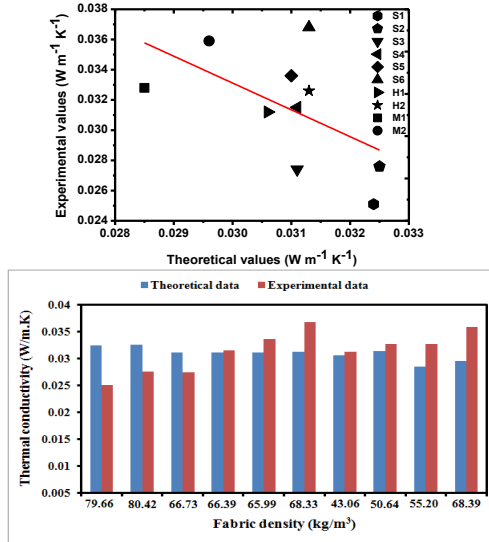


Figure 7: Thermal conductivity - alambda (Experimental data Vs Theoretical model data).

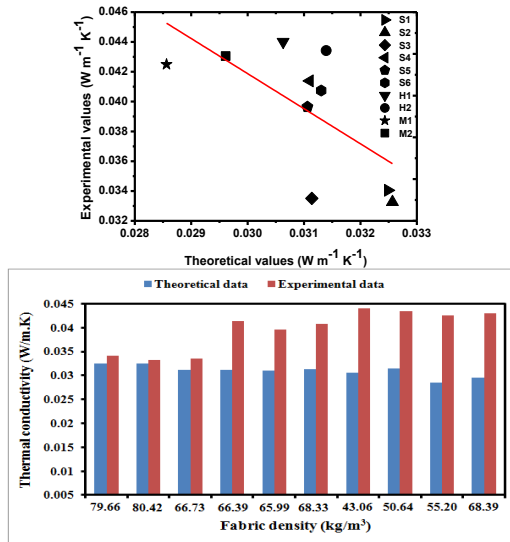


Figure 48: Thermal conductivity -TCi (Experimental data Vs Theoretical model data).

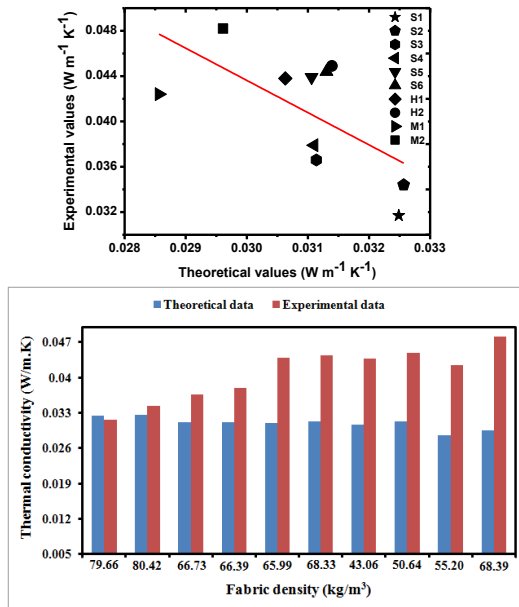


Figure 19: Thermal conductivity - custom built instrument (Experimental Vs Theoretical model data).

The thermal resistance values obtained from theoretical and experimental values are compared as shown in figure 20.

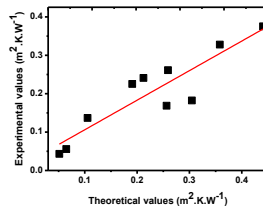


Figure 20: Thermal resistance (Experimental Vs Theoretical model data) for the case Alambeta

Convective Heat Transfer by Forced Convection - Laboratory setup Instrument

To predict the contribution of convective heat transmission on total thermal transmission characteristics of fabrics, the thermal resistances of fabrics were measured under forced convection mode. From the statistical analysis, it can be seen that the thermal transmission through multilayered fabrics significantly differs under convective mode of heat transfer. It can be observed from table 4 that the thermal resistance of all the fabrics under forced convection mode shows high thermal resistance. The thermal resistance during forced convection in general is lower than that of natural convection, because of higher air speed. So the heat transfer through fabric is generally higher. The thermal transmission during forced convection takes place due to the movement of air and the heat transfer coefficient depends on the air velocity [30-32]. It can be observed from table 4 that aerogel treated nonwoven fabrics has highest thermal resistance.

Table 4. Results of laboratory set-up instrument.

Samples	Temperature Gradient (Convection) °C	Heat Transfer Coefficient [W/(m ² K)]	Thermal conductivity [W/(mK)]	Thermal resistance [(m ² K)/W]x10 ⁻³
S1	14.5	26.31	0.0440	77.46
S2	9.0	30.60	0.0360	172.07
S3	8.3	28.52	0.0310	214.54
S4	10.0	27.07	0.0330	244.24
S5	12.5	25.81	0.0420	264.76
S6	7.5	29.25	0.0290	477.51
H1	6.8	38.38	0.0430	218.64
H2	6.5	32.71	0.0390	258.78

Note: “±” is the upper and lower 95% confidence interval of the mean.

The needle punched struto nonwoven fabrics show least thermal resistance value. The higher thermal resistance in aerogel treated nonwoven fabric is mainly due to presence of higher amount of air within the structure. The thermal resistance differs with respect to thickness of the fabrics used in the study. From the statistical analysis, it is observed that the type of fabric significantly affects the thermal resistance of multilayered fabrics. The effect of type of fabric on thermal resistance is statistically significant at 95% confidence interval. The thermal transmission at this situation is solely governed by the thermal resistance of the component fabric layer. The only difference between the fabrics H1 and H2 is the middle layer, i.e. meltblown polyamide nanofiber NF1 and NF2, respectively. It is also evident from table 4 that in general the thermal resistance of fabric H1 and H2 are lower than the S1 to S6. The reason for this is that the middle layer of the S1 to S6 fabric consists of aerogel with relatively higher thermal resistance than needle punched struto nonwoven fabric (H1 and H2). Convective heat transfer coefficient depends on air velocity, which defines the type of the convection [33]:

- for small air flow velocities ($V_a < 1$ m/s) there is a free convection type, for which:

$$h_c = 3.5 + 5.2 V_a \quad (8)$$

- for higher velocities ($V_a > 1$ m/s), the forced convection is as follows:

$$h_c = 8.7 V_a \quad (9)$$

Since fabrics were measured in forced convection mode, the heat transfer coefficient is calculated with air velocity 2.5 m/s. By substituting the air velocity in the equation 4.5, the heat transfer coefficient for forced convection is 21.75 W/(m²K).

Probability-Probability (P-P) plot compares data distribution with several theoretical models, using the empirical cumulative distribution function and cumulative distribution function of normal (solid blue curve), Laplace, and uniform distributions. A model which fits data well should plot approximately as the $y = x$ line. From the figure 21 the data fit well with $y = x$ line except sample H1 (conduction) which proves that the other samples have better fit. The plots are used to distinguish among symmetrical distributions according to their kurtosis. The parameters and values shown in table 5 are calculated for the fluid flow profile above the fabric samples. From these dimensionless numbers the type of flow can be found. For any given condition of velocity profile, it is the relative magnitude of ν/α which determines the magnitude of convective heat transfer.

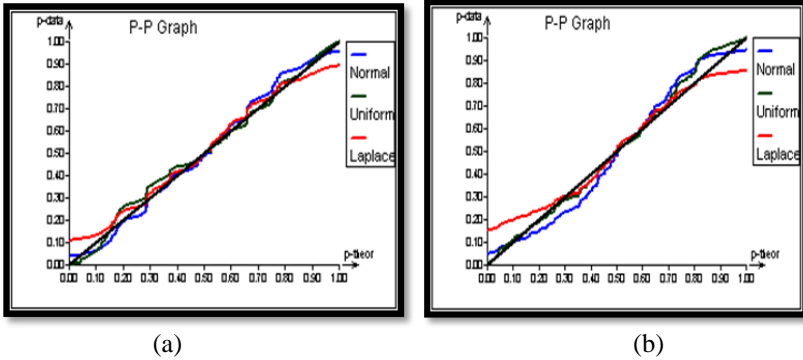


Figure 21: Probability-Probability (P-P) plot of Heat transfer (a) Convection
(b) Conduction

Table 5. Calculated parameters of the fluid flow profile.

The length of the specimen	$L = 15 \text{ cm}$
Area of the specimen	$A = 120 \text{ cm}^2$
Air free-stream velocity	$u_{\infty} = 2.5 \text{ m s}^{-1}$
Air free-stream temperature	$T_{\infty} = -10^{\circ}\text{C}$
Air viscosity	$\mu = 0.017 \text{ cP}$
Air density	$\rho = 1.29 \text{ kg m}^{-3}\text{K}^{-1}$
Air specific heat	$c_p = 1.005 \text{ kJ kg}^{-1}\text{K}^{-1}$
Thermal conductivity of air	$k = 0.025 \text{ W m}^{-1}\text{K}^{-1}$
Reynolds Number	$Re = 2.84 \times 10^3$
Prandtl Number	$Pr = 0.683$
Nusselt Number	$Nu = 139.8$
Heat Transfer Coefficient	$h_c = 23.3 \text{ W m}^{-2}\text{K}^{-1}$

Correlations between three important dimensionless (empirically obtained) numbers can be used to estimate the value of heat transfer coefficient. The convective heat transfer coefficient h_c strongly depends on the fluid properties and *roughness* of the solid surface, and the type of the fluid flow (*laminar* or *turbulent*).

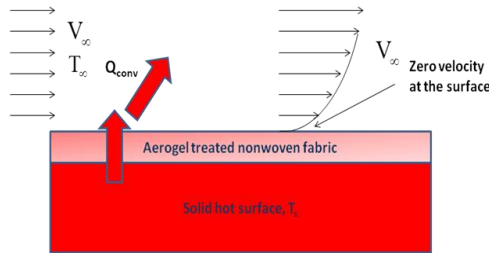


Figure 22: Forced convection.

As shown in the figure 22, it is assumed that the velocity of the fluid is zero at the wall; this assumption is called no slip condition. As a result, the heat transfer from the solid surface to the fluid layer adjacent to the surface is by pure conduction, since the fluid is motionless. The velocity and the temperature of the fluid approaching the fabric are uniform at U_∞ and T_∞ . The fluid can be considered as adjacent layers on top of each others.

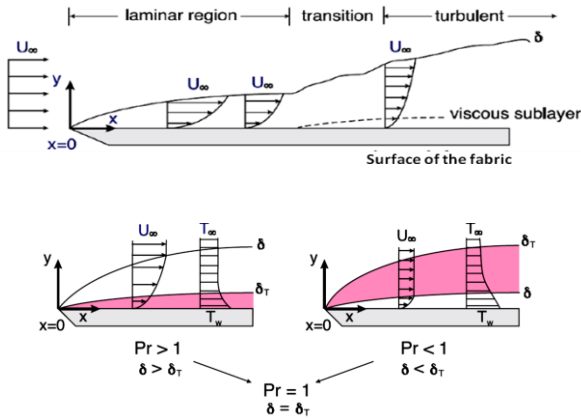


Figure 23: (Top) Velocity boundary layer. (Bottom) Thermal boundary layer.

Assuming no-slip condition at the wall, the velocity of the fluid layer at the wall is zero. The motionless layer slows down the particles of the neighboring fluid layers as a result of friction between the two adjacent layers. The presence of the fabric is felt up to some distance from the fabric beyond which the fluid velocity U_∞ remains unchanged. This region is called *velocity boundary layer* as shown in figure 23(a). Similar to velocity

boundary layer, a thermal boundary layer as shown in the figure 23(b) develops when a fluid at specific temperature flows over a surface which is at different temperature. The thickness of the thermal boundary layer δ_t is defined as the distance at which:

$$\frac{T - T_s}{T_\infty - T_s} = 0.99 \quad (10)$$

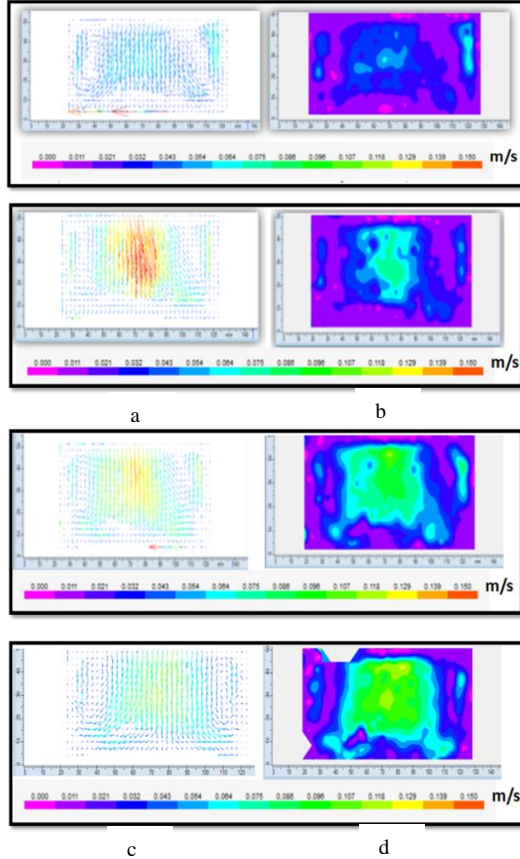


Figure 24: Vector and scalar maps for temperature gradient (a) 21.5°C (b) 23.8°C (c) 37.5 °C (d) 51.0 °C.

The relative thickness of the velocity and the thermal boundary layers is described by the Prandtl number. For low Prandtl number fluids, heat diffuses much faster than momentum flow ($Pr = \nu/\alpha \ll 1$) and the velocity boundary layer is fully contained within the thermal boundary layer. On the

other hand, for high Prandtl number fluids, i.e. oils, heat diffuses much slower than the momentum and the thermal boundary layer is contained within the velocity boundary layer.

Fluid Flow by Thermal Convection using Particle Image Velocimetry

Vector and scalar maps of the fluid flow developed by thermal convection above the textile sample were plotted for different temperature gradients. The vector maps are colored to highlight the acceleration zones. The scalar maps were put in one scaling and could be compared. Scalar maps are used to display the on-screen multiple data derived from the velocity fields. The x and y axis scales in vector and scalar maps illustrate the magnitude and direction of the out-of-plane velocity component.

Vorticity contours for the instantaneous flow structure is a vector field that gives a microscopic measure of the rotation at any point in the fluid. Vector and scalar maps for temperature gradients corresponding to difference between human body and chilling atmosphere are shown in figure 24. Evaluation recorded is based on the relationship between speed, distance, and time, where distance represents the displacement of particles entrained in the surrounding fluid (air) flowing in a defined time interval between two laser pulses.

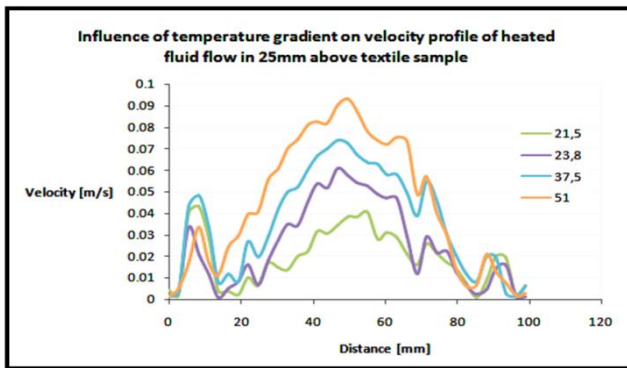


Figure 55: Distance and air velocity diagram.

The distance and air velocity diagram is shown in figure 25. These charts describe the behavior at different temperature gradients (between the textile sample and temperature of neighborhood). As it is expected, the fluid flow motion accelerates according to the increasing temperature gradient. This velocity profile is taken 25 mm above the free surface of the textile sample. The maximum velocity is reached with temperature gradient of 51.0 °C. The construction of the testing chamber did not allow observing the situation just

above the surface of textile sample due the reflections. These results are very important for setting the boundary condition of numerical simulation, describing the behavior of textile samples in the subzero temperature condition as well as for simulation of heat transfer through the porous media.

Modeling and Simulation of Heat Transfer Through Aerogel Treated Nonwoven Fabrics

During simulation in ANSYS, a constant ambient temperature of $-10\text{ }^{\circ}\text{C}$ was considered. Simulation was done so as to allow heat to flow along the thickness of the fabric (perpendicular to both the machine and the cross direction).

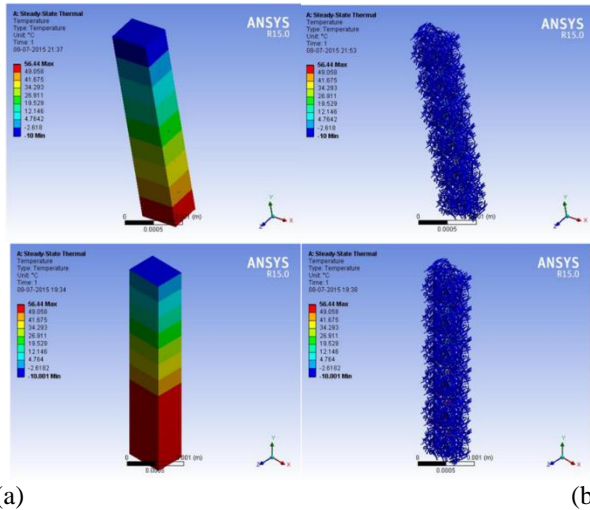


Figure 66: Temperature gradient for (a) standard nonwoven without aerogel; (b) aerogel treated nonwoven.

As the heat flows under the temperature gradient provided, various levels of the fabric thickness settle down to different equilibrium temperatures which is depicted in the ‘Temperature’ diagram shown in figure 26. Apart from this, variations in the ‘Total Heat Flux’ and the ‘Directional Heat Flux’ (along the Y axis – because that is the major direction for heat transfer) have been shown. Clearly, the heat retention in the nonwoven structure with aerogel is 67% higher than in the nonwoven structure without aerogel implying that aerogel hinders heat transfer, thus keeping the body warmer.

Using COMSOL, In the case of standard nonwoven without forced convection shown in figure 27(a), the temperature at the surface exposed to

outside air was 329.18955 K and the heat rate through the fabric was 2.185×10^{-8} W. In the case of standard nonwoven with forced convection showed in figure 27(b), the temperature at the surface exposed to outside air was 318.04327 K and the heat rate through the fabric was 1.024×10^{-8} W. In the case of nonwoven with aerogel and without forced convection shown in figure 27(c), the temperature at the surface exposed to outside air was 329.18949 K and the heat rate through the fabric was 1.267×10^{-8} W. In the case of nonwoven with aerogel and with forced convection shown in figure 27(d), the temperature at the surface exposed to outside air was 310.16686 K and the heat rate through the fabric was 9.801×10^{-9} W.

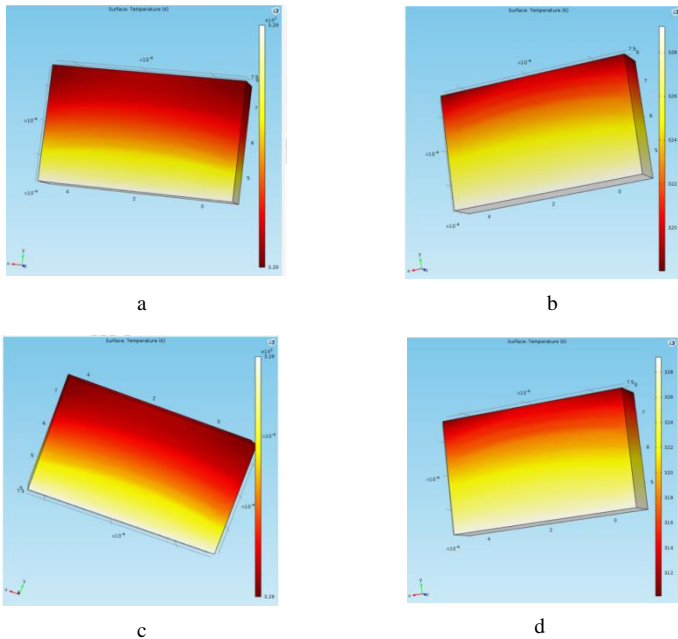


Figure 27: Heat transfer through (a) standard nonwoven without forced convection.(b) standard nonwoven with forced convection (c) aerogel treated nonwoven without forced convection (d) aerogel treated nonwoven with forced convection.

In the case of forced convection, the difference between the surface temperatures in case of air and aerogel for is almost 8 K even for such a small unit cell. When forced convection was not taken into account, the temperature difference was very less (6×10^{-5} K). But in both cases, the heat flow through air is higher than in case of aerogel. In the case with forced convection, the heat rate was around 5% higher and in the case without

forced convection, the heat rate was more than 72% higher. That is, the heat loss through the air is 1.7 times the heat loss through aerogel, in the case without any forced convection. The total net heat rate is defined as the net incoming and outgoing heat fluxes through all the surfaces of the body. This value for forced convection case is seen to be less in both aerogel and air because the outgoing flux is much more when there is a forced convection. The temperature versus length plot was also made. This was a smooth curve for the cases of forced convections but in the cases with no forced convections, the graph obtained had steps maybe because of very less variation of temperature in those regions.

Acknowledgement

This work was supported by the projects “Sophisticated hybrid tapes for fabrication of composites by precise winding” No. TJ01000292, 14014/136, and Design, optimization and application of smart heat-insulating nano-layers” No. LTACH-17014, 18301, Czech Ministry of Education, Czech Republic.

Conclusions

Objective measurement methods are required for accurate results in evaluation of heat transmission properties. In this study, various thermal measurement techniques were used and different types of insulation materials were characterized with regard to thermodynamical properties at different temperature gradients. It was observed that thermal conductivity of a fabric increases significantly with increases in the heating temperature. Thermal resistance (R_{ct}) of the fabric, which depends on the boundary layer of air, was directly proportionate to fabric thickness. The thermal resistance (R_{ct}) of the aerogel-treated nonwoven fabric was comparatively higher than other fabrics. Also, the air permeability was directly proportional to percentage of nanoporosity of the aerogel based composite structure. It was also noticed that, when the pressure level increases the flow rate also increases simultaneously. The relationship between the temperature gradient (between the textile sample and temperature of neighborhood) and velocity of fluid flow was described from the PIV measurements. As expected, the fluid flow motion accelerated according to the increasing temperature gradient. The custom built instrument and the laboratory set-up equipment were found to be effective in measuring the heat transport properties of fabrics as they measure the steady-state thermophysical properties (thermal insulation properties) even at sub-zero temperatures. Thus, the fabric density and the aerogel present in the structures have a significant effect on thermal

properties of aerogel-treated nonwoven fabrics. In general, greater the fabric thickness, greater the thermal insulation. It concludes that the selected aerogel treated fabrics have high thermal performance and thermal response as insulators as compared with other fabrics. The simulations on ANSYS and COMSOL confirmed that thermal behavior of the fabric improved when treated with aerogel. There was good agreement between simulation and experimental data. The newly fabricated and designed instruments were found to be suitable to measure conductivity and convection at sub-zero temperatures and convenient for the measurement and evaluation of various temperature variations at different positions of the fabric. This method of measurement still needs optimization and will be the subject of further research.

References

- [1] S. Varkiyani, H. Rahimzadeh and H. Bafekrpoor, "Influence of punch density and fibre blends on thermal conductivity on nonwoven", *Open Textile Journal* (4), 1-6 (2011).
- [2] E. Cohen, "Thermal properties of advanced aerogel insulation", in *Department of Mechanical Engineering. Massachusetts Institute of Technology, Massachusetts* (2011).
- [3] A.D Gun, "Dimensional, Physical and Thermal Comfort Properties of Plain Knitted Fabrics Made from Modal Viscose Yarns Having Microfibers and Conventional Fibers", *Fibers and Polymers* 12(2), 258-267 (2011).
- [4] N. Mao and S.J Russell, "The thermal insulation properties of spacer fabrics with a mechanically integrated wool fiber surface", *Textile Research Journal* (77), 914-922 (2007).
- [5] "Heat & Mass Transfer in Textiles", *World Scientific and Engineering Academy and Society*, ed. A. HAGHI, Montreal, Canada (2011).
- [6] J. Fricke, "Thermal transport in porous superinsulations", *Aerogels, Springer Proceedings in Physics* (1986).
- [7] Z. Novak and Z. Knez, "Diffusion of methanol-liquid CO₂ and methanol-supercritical CO₂ in silica aerogels", *Journal of NonCrystalline Solids* 221(2-3), 163-169 (1997).
- [8] H. Tamon, T. Kitamura and M. Okazaki, "Preparation of silica aerogel from TEOS", *Journal of Colloid and Interface Science* 197(2), 353-359 (1998).
- [9] Y. Li, M. Plante and B.V. Holcombe, "Fibre hygroscopicity and perceptions of dampness part-II: Physical mechanisms", *Textile*

- Research Journal (65), (1995).
- [10] S.S. Kistler, "Coherent expanded-aerogel", *Journal of Physical Chemistry* (36), 52-64 (1931).
- [11] T. Xie, Y.L. He and Z.J. Hu, "Theoretical study on thermal conductivities of silica aerogel composite insulating material", *International Journal of Heat and Mass Transfer* (58), 540-552 (2013).
- [12] A.S. Dorcheh and M.H. Abbasi "Silica aerogel; synthesis, properties and characterization", *Journal of Materials Processing Technology* 199(1), 10-26 (2008).
- [13] B. Hosticka, P.M. Norris, J.S. Brenizer and C.E. Daitch, "Gas flow through aerogels", *Journal of Non-Crystalline Solids* 225(1-3), 293-297 (1998).
- [14] D. Bhattacharjee and V. K. Kothari, "Measurement of Thermal Resistance of Woven Fabrics in Natural and Forced Convections", *Research Journal of Textile and Apparel* 12(2), (2008).
- [15] M. Milan and J. Militky, *Statistical Data Analysis*, (Woodhead Publishing, New Delhi, 2011), pp. 763.
- [16] M. Kelnberger and G. Schwitzgebel, "Application of single oscillator double pulse laser systems for Particle Image Velocimetry", *Erschienen in Laurin Photonics Handbook*, (Innolas GmbH, Krailling, Germany, 2005)
- [17] M. Raffel, C.I. Willert, S.T. Wereley and J. Kompenhans, *Particle Image Velocimetry 2nd Edition*. (Springer-Verlag Berlin Heidelberg, 1998).
- [18] M.M. Dubinin, "Theory of physical adsorption of gases and vapors and the adsorption properties of some adsorbents differing in nature and having a porous structure", *Izvestiya Akademii Nauk SSSR. Seriya Khimicheskaya* (7), 1153-1161 (1960).
- [19] M.M. Dubinin, "The potential theory of adsorption of gases and vapors for adsorbents with energetically nonuniform surfaces" *Chemical Reviews* (60), 235-241 (1960).
- [20] IUPAC Manual of Symbols and Terminology, Appendix 2, Pt.1, Colloid and Surface Chemistry. *Pure Applied Chemistry* (31), 578 (1972).
- [21] P. Lizak, "Structure of yarn and its influence on properties of fabrics", *Vlakna a Textil* 4, 213-221 (1998).
- [22] Z.S. Abdel-Rehim, M. Saad, M. El-Shakankery and I. Hanafy, "Textile fabrics as thermal insulators", *Autex Research Journal* (6), 148-161 (2006).
- [23] M. Mohammadi and L.P. Banks, "Determining effective thermal conductivity of multilayered nonwovens fabrics", *Textile Research Journal* (73), 802-808 (2003).
- [24] P.L. Houston, *Chemical kinetics and reaction dynamics*. (Dover, New York, 2007).
- [25] L.W. Hrubesh, "Aerogel applications" *Journal of Noncrystalline Solids* (225), 335-342 (1998).

- [26] W.A. Lotens, "The actual insulation of multilayer clothing", *Scandinavian Journal of Work Environment & Health* 15(1), 66-75 (1989).
- [27] K. Slater, "Comfort properties of textiles", *The Textile Institute*, 1-11 (1977).
- [28] Y. Li and B.V.Holcombe, "Mathematical Simulation of Heat and Moisture Transfer in a Human-Clothing-Environment System", *Textile Research Journal* 68(6), 389-397 (1998).
- [29] M.N. Ozisik, *Heat transfer – A basic approach*. (McGraw Hill, New York, 1985).
- [30] ASHRAE - *Handbook of Fundamentals*. (American Society of Heating, Refrigerating and Air-Conditioning Engineers Inc., TN, 1977).
- [31] R.J. Kind, J.M. Jenkins and C.A Broughton, "Measurements and prediction of wind-induced heat transfer through permeable cold-weather clothing" *Cold Regions Science and Technology* 23(4), 305–316 (1995).
- [32] W.F.Stoecker and J.W. Jones, *Refrigeration and air conditioning Vol. 2*. (McGraw-Hill Book Company, Singapore, 1982).
- [33] M. Konarska, K. Sołtynski, I. Sudoł-Szopińska and A. Chojnacka, "Comparative Evaluation of Clothing Thermal Insulation Measured on a Thermal Manikin and on Volunteers", *Fibres & Textiles in Eastern Europe* 15(2), 61 (2007).